Hydrodynamic Assist of Dynamic Wetting

Terence D. Blake and Andrew Clarke
Research Division, Kodak Limited, Harrow HA14TY, England

Kenneth J. Ruschak
Manufacturing Research and Engineering, Eastman Kodak Co., Rochester, NY 14652

Dynamic wetting speeds are limited by the gross entrainment of air between the liquid and the moving substrate. We present experimental data for the curtain-coating method, in which liquid impinges at high speed on the substrate. We also show that air entrainment is strongly affected by macroscopic hydrodynamics and is subject to hysteresis. Using boundary-layer theory, a simple hydrodynamic model is developed for the flow field in the impingement zone away from the dynamic wetting line. The model approximately accounts for the shear thinning of polymer solutions and for the influence of surface tension. We apply the molecular kinetic theory of dynamic wetting, modified to account for hydrodynamic stress, to the immediate vicinity of the wetting line. The main result is a correlation for air-entrainment data.

The experimentally calibrated model predicts that the hydrodynamic assist of wetting is greatest when the dynamic wetting line is located beneath the impinging curtain. Flow visualization supports this physical picture.

Introduction

Dynamic wetting is central to many physical processes. An ambient fluid, often air, in contact with a solid is displaced by a liquid. At sufficiently high displacement speeds, wetting failure occurs, and the ambient fluid is entrained between the liquid and the solid. Usually dynamic wetting failure has undesirable consequences, and in the case of coating operations, for example, air entrainment limits processing speed.

Dynamic wetting has been most frequently studied by plunging a solid into a relatively large, stagnant pool of liquid (for example, Perry, 1967; Inverarity, 1969; Burley and Kennedy, 1976; Gutoff and Kendrick, 1982; Burley and Jolly, 1984; Blake, 1988; Brache et al., 1989; Seebergh and Berg, 1992). The angle at which the interface intersects the solid, as viewed through a low-power microscope or inferred from measurement of meniscus shape or force exerted on the solid, is determined as a function of speed. At low magnification, the interface appears to intersect the solid as a line, and the angle measured through the liquid is termed the apparent or macroscopic dynamic contact angle.

At the lowest speeds, the contact angle approaches the static advancing contact angle. The contact angle increases as speed is increased, with the wetting line remaining straight and horizontal (that is, normal to the velocity of the solid). However, when the angle reaches a nominal value of 180°, wetting failure occurs, and a thin film of air, on the order of a micron in thickness (Perry, 1967), forms between the liquid and solid. The wetting line moves downward, becomes unsteady, and breaks up into straight-line segments that are inclined from the horizontal. The angle of inclination increases steadily with speed. At any instant, the wetting line has the appearance of sawteeth (Burley and Kennedy, 1976; Blake and Ruschak, 1979; Burley, 1992), and air bubbles may be formed at the downstream vertices of the sawteeth and carried into the liquid. The speed at which wetting failure begins varies inversely with viscosity raised to a power of about 0.7. Speed can also vary about a factor of 5 due to the chemical and physical properties of the solid (Buonopane et al., 1984; Blake and Ruschak, 1994).

The case where only one sawtooth, having one vertex, forms is rare but particularly instructive. The wetting line then consists of two slanted and *steady* straight-line segments in the shape of a "V." Blake and Ruschak (1979) showed that the component of the speed of the solid normal to the segments is a constant that they termed the maximum speed of wetting. Initially, no air bubbles are produced, but as speed and the

Correspondence concerning this article should be addressed to K. J. Ruschak.

inclination angle increase, air bubbles begin to form at the vertex. At still higher speed, an air tube may form and persist for a significant distance before breaking up. The vertex may be several centimeters downstream of the level of the pool, and over this distance the liquid is separated from the solid by a thin, triangular-shaped layer of air contained within the "V"-shaped wetting line. As speed is decreased, the inclination angle decreases until the wetting line is once again horizontal. The air film appears to recede rather than collapse.

There is almost no published data for the onset of air entrainment in flows other than a solid plunging into a pool, although the speed can be markedly different. In the present work, we study dynamic wetting using the curtain-coating method. Curtain coating is used for applying cosmetic or protective finishes to a variety of substrates and for forming the functional layers of products like photographic film. Brown (1961) and Kistler (1983) used curtain coating to study air entrainment on a prewetted solid surface. The essence of this method is that the liquid impinges on the solid as a two-dimensional jet. In this context, the word "curtain" means a vertical sheet of liquid, accelerated by free fall. Curtain coating is an ideal flow for observing macroscopic hydrodynamic effects on dynamic wetting. Inertial effects are more important than in the plunging flow. Moreover, the impact of the curtain on the solid generates a pressure that, we believe, can postpone the formation of an air film to higher speed.

We develop a simple hydrodynamic model for the macroscopic flow based on boundary-layer theory. The model allows us to predict the position of the wetting line. The position of the wetting line relative to the surfaces of the curtain turns out to be useful in interpreting and correlating experimental data. This model cannot speak to events in the immediate vicinity of the dynamic wetting line. We choose to apply the molecular theory of dynamic wetting, as recently modified to include the effect of hydrodynamic stress, to suggest how the correlation of the data can be completed.

After describing the experimental method, we present experimental data and observations for aqueous solutions of several polymers. The end result is a complete correlation of the experimental data, which leads to the conclusion that the hydrodynamic assist of dynamic wetting is greatest when the wetting line is located beneath the impinging curtain. In this situation, air entrainment speed increases almost linearly with the component of the impingement speed normal to the solid. There is no quantitative precedent in the literature for the effect of the impingement speed. Optical cross-sections of the flow support this physical picture of the macroscopic hydrodynamic assist of wetting.

Background

Since air entrainment commences when the apparent dynamic contact angle approaches 180°, the factors that affect the dynamic contact angle are central to dynamic wetting failure. Although the dynamic contact angle has been studied extensively, there is no complete and experimentally verified model. One general approach is to view the dynamic contact angle as a generalization of the static contact angle and attribute the difference between the static and dynamic contact angles to an upset at the wetting line of thermodynamic equilibrium, described classically by Young's equation. The molecular kinetic theory of dynamic wetting is based upon the methods developed by Eyring and others (Glasstone et al., 1941) and attributes the velocity dependence of the contact angle to the disturbance of adsorption equilibria at the wetting line. Wetting line movement is modeled statistically as a stress-modified rate process composed of individual molecular displacements (Cherry and Holmes, 1969; Blake and Haynes, 1969; Blake, 1988). The driving force that alters the energy barriers to molecular displacements, so that the wetting line can move, has components arising from both surface tension and viscous shear stress. The model has been shown to fit well dynamic contact angle data from plunging experiments up to capillary numbers of about 0.1. At higher capillary numbers, hydrodynamic effects must evidently be taken into account (Blake, 1988; Blake, 1993).

A second general approach, first investigated by Hansen and Toong (1971), attributes much or all of the difference between the static and dynamic contact angles to hydrodynamic bending of the meniscus so close to the wetting line as not to be visible. Voinov (1976) and many others including Dussan V. (1976), Dussan V. (1979), Hocking and Rivers (1982), Huh and Mason (1977), Cox (1986), and de Gennes et al. (1990) have analyzed the hydrodynamics. The apparent and submicroscopic contact angles then differ appreciably, but this has yet to be directly observed or indisputably inferred. A submicroscopic contact angle is required. When that is taken to be the static contact angle (for example, Hocking and Rivers, 1982), all of the variation of contact angle with speed is attributed to hydrodynamic bending of the interface on a submicroscopic scale. It is not clear that this choice for the submicroscopic contact angle is generally appropriate, however (Blake and Ruschak, 1994). Petrov and Petrov (1992) have suggested using molecular-kinetic theory to provide a speed-dependent submicroscopic contact angle.

At very low speeds, the macroscopic contact angle approaches the advancing static angle and so is dominated by surface forces. The static contact angle is used as a boundary condition in problems of capillary hydrostatics, and the flow of information is outward from the contact line. Hydrodynamics must eventually play a role in determining the apparent angle as speed is increased. The first role may indeed be a bending of the meniscus on a submicroscopic scale, a local effect that may be the same or similar for most flow geometries. Under more extreme conditions, however, the macroscopic hydrodynamics can be expected to influence the apparent contact angle. Indeed, in the (singular) limit of vanishing surface tension, the apparent dynamic contact angle can be computed from the equations of hydrodynamics alone, without reference to the local conditions at the wetting line (Kistler, 1983), as the flow of information reverses and is toward the wetting line. So, high Weber and capillary numbers favor macroscopic hydrodynamic control of the apparent contact angle. When these numbers are of order unity, both surface and macroscopic hydrodynamic forces may contribute to the apparent contact angle.

Two-dimensional models for the air film that forms as the dynamic contact angle approaches 180° have been developed by Perry (1967) and Teletzke, Davis and Scriven (1988). The latter considered the collapse of an entrained air film due to long-range molecular forces modeled as disjoining pressures. The model predicts that a thin film of air separates the liquid

and solid at all but the lowest speeds; this air film is unstable and subsequently breaks up and is absorbed (Miyamoto, 1991). Mues, Hens and Boiy (1989) have provided some indirect experimental support for this hypothesis.

However, the existing theories for an air film fail to account for the strong effect of the viscosity of the liquid seen in experiments. The theories may not be consistent with the observed sudden onset of the sawtooth wetting line and entrained air bubbles. Blake and Ruschak (1994) have proposed that the air film does not collapse with decreasing speed, but instead retreats. This notion is based on the sawtooth shape of the wetting line, and the fact that the speed of the solid normal to the segments of the wetting line, what Blake and Ruschak (1979) termed the maximum speed of wetting, is independent of speed. As the speed of the solid is decreased, the angle of inclination of the wetting line segments decreases, and the extent of the air film shrinks until the wetting line is straight. So viewed, air entrainment is inherently a three-dimensional phenomenon that cannot be explained by two-dimensional models. An air film will always form once the contact angle reaches 180° because of the large lubrication pressures developed in the air (Blake and Ruschak, 1994). Since the appearance and disappearance of the air film are directly determined by the maximum speed of wetting, the strong effect of the viscosity of the liquid seen in experiments is explained.

Most experimental studies of air entrainment are for a solid plunging into a large pool of liquid. There are three observations which support the notion that macroscopic hydrodynamics plays a secondary role in this flow: air entrainment occurs before the capillary number exceeds about one; air-entrainment speed does not depend on the angle of entry (Burley and Jolly, 1984); and the component of the speed of the solid surface normal to the sawtooth wetting line remains constant (Blake and Ruschak, 1979). In curtain coating, on the other hand, the speed of air entrainment is sensitive to flow rate, impingement speed, and impingement angle. At the base of the curtain, the Weber number typically exceeds two, and surface waves are washed downstream (Lin, 1981); the apparent contact angle is not likely to be dominated by events near the contact line in this case. When the Weber number is less than two, the trajectory of the curtain is sensitive to the apparent contact angle and no longer lies in a vertical plane. Our experimental results do not include Weber numbers below two because the curtain is prone to disintegration and air entrainment speeds are low.

Description of the Flow

A vertical, two-dimensional sheet of liquid impinges on a substrate moving at speed S (Figure 1). The liquid has density, ρ, viscosity μ, and surface tension σ. The velocity profile in the curtain is that of plug flow, and the impingement speed, U, is on the order of 1 m/s. The substrate is inclined to the horizontal at an angle α, which is positive when the substrate has a positive component of velocity downward. The angle between the velocities of the curtain and substrate is $(\pi/2-\alpha)$. The volumetric flow rate per unit width is q, and so the thickness of the curtain, W, equals q/U. The ratio of the speed of the curtain to the speed of the substrate, U/S, is denoted δ and is typically less than unity in practice. All the liquid supplied by the curtain is entrained by the substrate, and a film of uniform thickness $D=q/S$ is formed.

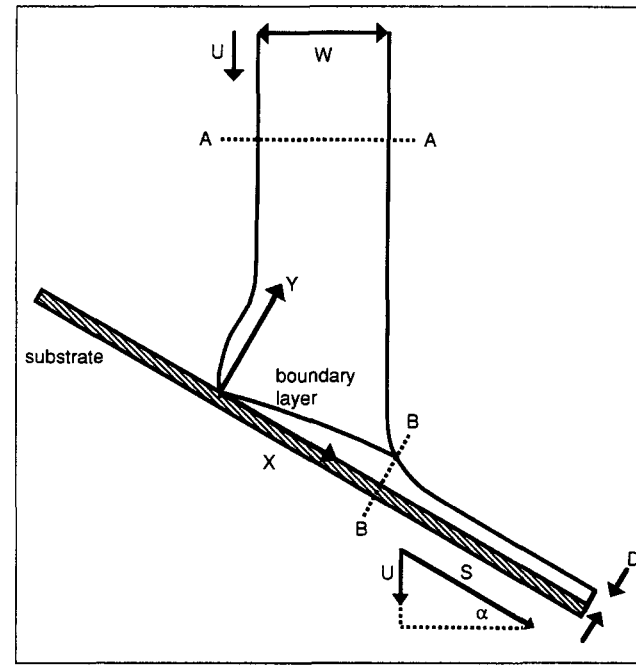

Figure 1. Flow.

An X-Y Cartesian coordinate system is introduced, for which the abscissa is in the plane of the substrate and the origin is at the dynamic wetting line where the liquid first appears to contact the substrate. Pressure is denoted P.

Usually, gravity is employed to accelerate the liquid. It is often a good approximation to neglect the effect of viscosity and consider the liquid to be in free fall (Brown, 1961). If U_0 is the initial speed of the curtain, G is the gravitational acceleration, and H the vertical drop to the substrate, then the impingement speed is given by:

$$U=\sqrt{U_0^2+2GH} \tag{1}$$

When H exceeds a few centimeters, the effect of U_0 on the impingement speed is negligible.

Analysis of the Flow

Boundary layer analysis

The flow field for curtain coating is not very complicated, and we try to capture its essential features in a relatively simple model that can be used to correlate and interpret experimental data. Gross properties of the flow can explain much of what is experimentally observed. A detailed theory for the onset of air entrainment must await further progress on theory for the dynamic contact angle. Our main objective is to estimate the location of the dynamic wetting line, and to that end we concentrate on the boundary layer of entrained liquid adjacent to the substrate. Liquid outside the boundary layer has not felt the viscous stresses arising from the motion of the substrate. At first, we consider the liquid to be Newtonian. We develop and extend the boundary layer analysis of Sakiadis (1961a,b). Using the finite-element method, Kistler (1983) computed the flow field in curtain coating for the case of a horizontal substrate in the singular limit of no surface tension; he showed

that the analysis of Sakiadis predicts boundary-layer length well for that case.

The boundary layer (Figure 1) begins at the dynamic wetting line, where the liquid contacts the substrate, and grows in thickness until all of the supplied liquid has been entrained. The end point of the envelope of the boundary layer must lie on the streamline running along the downstream (front) surface of the curtain, and we assume that it lies on that surface. If the point were located internally, there would be a region of recirculation adjacent to the downstream surface of the curtain, and this is not the case under the conditions considered. This physical picture is supported by detailed computer simulations of the flow field (Kistler, 1983) and by flow visualization, examples of which are offered below. Thus, the length of the boundary layer gives, in effect, the distance of the dynamic wetting line behind the front surface of the curtain.

For flow in the boundary layer, the X-component of velocity is scaled with S, the Y-component with U, and the pressure with ρU^2. The Y-coordinate is scaled with D, the film thickness far downstream, and the X-coordinate with the thickness of the curtain, W. With u and v the dimensionless velocity components, p the dimensionless pressure, and x and y the dimensionless coordinates, the Navier-Stokes and continuity equations can be written for steady flow as:

$$Re(uu_x + vu_y) = -Re\delta^2 p_x + u_{yy} + \delta^2 u_{xx} \tag{2}$$

$$Re(uv_x + vv_y) = -Re\, p_y + v_{yy} + \delta^2 v_{xx} \tag{3}$$

$$u_x + v_y = 0 \tag{4}$$

Here, Re is a Reynolds number, $\rho UD/\mu$. The no-slip condition at the surface of the substrate gives boundary conditions on u and v:

$$u = 1 \quad (y = 0) \tag{5}$$

$$v = 0 \quad (y = 0) \tag{6}$$

We consider the limiting case $\delta \ll 1$; that is, the speed of the substrate significantly exceeds the speed of the curtain. This implies that the final film thickness is much less than the thickness of the curtain. In this situation, Eqs. 1 and 2 reduce to boundary-layer form:

$$Re(uu_x + vu_y) = u_{yy} \tag{7}$$

$$Re(uv_x + vv_y) = -Re\, p_y + v_{yy} \tag{8}$$

An additional boundary condition is needed to close the problem, and we use:

$$u \to \delta \sin(\alpha) \quad (y \to \infty) \tag{9}$$

In other words, the x-component of velocity outside the boundary layer approaches the x-component of the curtain impingement velocity. The rationale for this choice is given below.

We solve Eqs. 4 and 7 for u and v, subject to conditions 5, 6 and 9. First, we introduce a stream function ψ to satisfy Eq. 4.

$$u = \psi_y \tag{10}$$

$$v = -\psi_x \tag{11}$$

We then use the standard similarity transformation to reduce the problem to an ordinary differential equation:

$$z = \sqrt{\frac{Re}{x}}\, y \tag{12}$$

$$\psi = \sqrt{\frac{x}{Re}}\, F(z) \tag{13}$$

Thus, the problem becomes:

$$F_{zzz} + \frac{1}{2} F F_{zz} = 0 \tag{14}$$

$$F = 0 \quad (z = 0) \tag{15}$$

$$F_z = 1 \quad (z = 0) \tag{16}$$

$$F_z \to \delta \sin(\alpha) \equiv \varphi \quad (z \to \infty) \tag{17}$$

The differential Eq. 14 allows F_z to approach a constant as z tends to infinity, and so it is possible to satisfy Eq. 17.

Rigorously, the behavior of u at infinity comes from matching the boundary layer solution with the solution valid outside the boundary layer. To consider the flow outside the boundary layer, we scale the X and Y coordinates with W, the velocity components with U, and the pressure with ρU^2. The viscous terms in the Navier-Stokes equation are then of order δ compared to the inertial and pressure gradient terms, and so to a first approximation the outer flow is determined by the equations for inviscid flow. The X-component of velocity in the inviscid flow is of order δ compared to that in the boundary layer. Thus, at lowest order in the boundary layer, it is not necessary to solve the flow outside the boundary layer, as matching requires that $u \to 0$ as $y \to \infty$. At order δ in the boundary layer, however, it is necessary to consider the flow outside the boundary layer. That problem is formidable, however, and instead of solving it we assume that the similarity solution for the boundary layer can match with the outer flow at order δ. The similarity solution requires that u tends to a constant of order δ as $y \to \infty$, and it is the outer, inviscid flow that determines this constant.

We infer what that constant must be from a balance of X-momentum. At the inlet of the control volume, which is a cross-section of the curtain some distance above the boundary layer (A-A in Figure 1), the flux of X-momentum is $\rho qU \sin(\alpha)$. The outlet of the control volume is the envelope of the boundary layer, which on the outer scale collapses to the surface of the substrate. The boundary layer draws in liquid (the Y-component of velocity varies as $-1/\sqrt{X}$), and the integral of the Y-component of velocity along the length of the boundary layer is $-q$. As a result, the constant value of the X-component of velocity at the boundary layer must be $U \sin(\alpha)$. The similarity solution can be viewed as a reasonable approximate solution in the event that it cannot be rigorously matched with

the outer flow at order δ. Our main interest is the position of the wetting line, an integral property of the flow, rather than the detailed flow field.

The nonlinear, ordinary differential Eq. 14 can be solved by numerical integration, but we choose to find an approximate solution that is easy to use. Let the envelope of the boundary layer be given by $z=\zeta$; at this location u has nearly reached its asymptotic value. We approximate F using a third-degree polynomial:

$$F=\frac{(1-\varphi)}{3\zeta^2}(z^3-3\zeta z^2)+z \quad (z\le\zeta) \tag{18}$$

This function satisfies the boundary conditions 15 and 16. Moreover, at $z=\zeta$ its slope is φ and its curvature is zero, and so there is a smooth connection with the straight line of slope φ which approximates F for $z>\zeta$ (see Eq. 17). The constant ζ is determined by satisfying the differential Eq. 14 in the mean:

$$\int_0^\infty \left(F_{zzz}+\frac{1}{2}FF_{zz}\right)dz=0 \tag{19}$$

Carrying out the integration gives:

$$\zeta=2\sqrt{\frac{15}{3+2\varphi}} \tag{20}$$

and as a result:

$$F(\zeta)=\frac{2}{3}(1+2\varphi)\sqrt{\frac{15}{3+2\varphi}} \tag{21}$$

The final step in the analysis is to compute L, the length of the boundary layer, by equating the flow rate in the boundary layer to q.

$$\frac{L}{D}=\frac{3}{20}\frac{(3+2\varphi)}{(1+2\varphi)^2}\left(\frac{\rho q}{\mu}\right) \tag{22}$$

For the case $\varphi=0$, the coefficient of $\rho q/\mu$ as given by this expression is 0.45; numerical solution of this special case by Sakiadis (1961b) gives 0.383. We also note that Sakiadis obtained a more accurate approximate solution by using a fourth-degree polynomial. Sakiadis did not solve the problem for boundary condition 17.

With the velocity field so determined, Eq. 8 can be readily solved for the pressure field in the boundary layer.

Relative wetting line position

We use the result for boundary-layer length, Eq. 22, to compute a dimensionless ratio that we term the relative wetting line position:

$$l=\frac{L}{W/\cos(\alpha)} \tag{23}$$

$W/\cos(\alpha)$ is the thickness of the curtain measured in a plane that is parallel to the substrate. Thus, for $l=1$, the dynamic wetting line lies in the plane of the rear surface of the curtain. When l is small, the wetting line is near the front surface of the curtain, and when l exceeds unity, the wetting line is to the rear of the curtain. Figure 2 illustrates the physical picture. When Eq. 22 is used for boundary layer length, it may be combined with Eq. 23 to give the relative wetting line position:

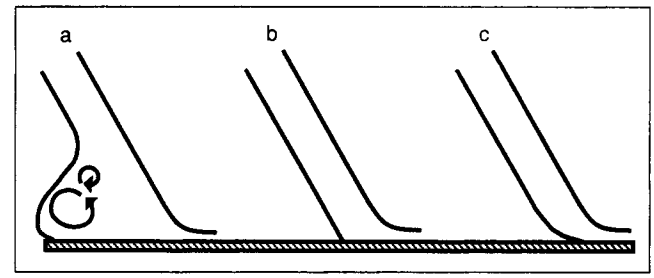

Figure 2. Relative wetting line position.
(a) greater than unity; (b) unity; and (c) less than unity.

$$l=\frac{3\delta}{20}\frac{(3+2\varphi)}{(1+2\varphi)^2}\cos(\alpha)\left(\frac{\rho q}{\mu}\right) \tag{24}$$

It is established below that the relative wetting line position is an effective parameter for correlating experimental data for the onset of air entrainment. We offer some thoughts towards an explanation of this finding.

The pressure generated as the curtain strikes the substrate can act as a load that may delay the establishment of an air film. We use a balance of Y-momentum to estimate the pressure imposed on the boundary layer. One surface of the control volume is a cross-section of the curtain above the substrate (A-A in Figure 1), and the flux of Y-momentum is $\rho q U\cos(\alpha)$. Another surface of the control volume is at the envelope of the boundary layer, which is virtually along the surface of the substrate when δ is small. The average value of the Y-component of velocity at this surface is q/L, where L is boundary layer length. If P is the average pressure along this surface, then conservation of Y-momentum gives the estimate:

$$P\approx\frac{\rho q U\cos(\alpha)}{L}-\frac{\rho q^2}{L^2} \tag{25}$$

The largest positive value for P is $(\rho/4)[U\cos(\alpha)]^2$, corresponding to $L=2W/\cos(\alpha)$, or $l=2$. This simple argument suggests that the relative wetting line position has an optimum value near unity for maximizing pressure and introduces the component of impingement speed normal to the substrate, $U\cos(\alpha)$, as a characteristic speed that may relate to the onset of air entrainment.

We suggest, then, that hydrodynamic effects will be most favorable for excluding an air film when the wetting line is near the plane of the rear surface of the curtain; that is, when the relative wetting line position is of order unity, as in Figure 2b. If l is large, as in Figure 2a, the wetting line is effectively isolated from the curtain by the large heel and accompanying recirculation regions which form in this situation (see Figure 11). Therefore, hydrodynamic effects on the wetting line are relatively weak, and we find experimentally that the speed at

the onset of air entrainment is low and roughly constant. For small l (Figure 2c), liquid speed remains high through the impingement zone and pressure is not increased near the wetting line. The situation geometrically favors an apparent dynamic contact angle of 180°, and hence air entrainment, because the rear surface of the curtain curves towards the front surface, resulting in a shallow angle of approach to the substrate.

Estimating the effect of shear-thinning

Shear rates in the boundary layer at the speeds approaching air entrainment can be on the order of 100,000/s. Most practical coating liquids, and in particular the solutions of high polymers used in our experiments, are non-Newtonian under such circumstances.

The rheology of polymer solutions can be complex. At the very least, solutions of high polymers become pseudoplastic, or shear-thinning, and this will affect the shear flow in the boundary layer. Some polymer solutions become significantly elastic as well. Only pseudoplastic behavior is considered here.

In the usual manner, an apparent Newtonian viscosity can be defined whose value decreases as shear rate increases. We take the simplest possible approach. First, an average or representative shear rate is calculated for the boundary layer. Second, the apparent Newtonian viscosity corresponding to this shear rate is determined. Finally, the apparent Newtonian viscosity is used to estimate the boundary-layer length using Eq. 22.

For most liquids, the apparent Newtonian viscosity becomes constant at sufficiently low rates of shear; the low-shear viscosity will be denoted μ_0. Once the liquid begins to shear-thin, it often follows power-law behavior; that is, the apparent viscosity varies as the shear rate raised to some power. At sufficiently high rates of shear, the apparent Newtonian viscosity may again become independent of shear rate. This second "Newtonian" viscosity will be denoted μ_∞.

The Carreau equation provides a simple, empirical model for such behavior (Bird, Amstrong and Hassager, 1987)

$$\frac{\mu-\mu_\infty}{\mu_0-\mu_\infty}=\frac{1}{[1+(\lambda\dot{\gamma})^2]^{(1-n)/2}} \tag{26}$$

Here μ is the apparent viscosity at shear rate $\dot{\gamma}$, λ is a characteristic relaxation time, and n is the power-law index. Often, the apparent viscosity cannot be measured at shear rates high enough for μ_∞ to be determined. Also, μ may remain considerably larger than μ_∞, which in many cases is of the same magnitude as the viscosity of the solvent, and it is then adequate to approximate μ_∞ as zero. Such is the case in the experiments reported here, and so the liquids are characterized by just three parameters: μ_0, λ, and n.

The representative shear rate for the boundary layer is:

$$\dot{\gamma}=[S-U\sin(\alpha)]/D \tag{27}$$

The quantity $[S-U\sin(\alpha)]$ is the velocity difference across the boundary layer, according to the analysis above. The final film thickness D is representative of the thickness of the boundary layer.

Effect of surface tension

Although surface tension has not been included in the analysis, it has a significant effect on the relative wetting line position for some of our data. In particular, we need to correct for the effect of surface tension when we compare calculated values of the relative wetting line position with observed values. Surface tension should be important when the Weber number, $We=\rho qS/\sigma$, is of order unity or smaller.

Because of the expected curvatures of the interfaces near the boundary layer (Figure 1), we expect surface tension to increase pressure where the boundary layer begins and decrease pressure where the boundary layer ends. Consequently, there should be a negative pressure gradient that shortens boundary-layer length.

We can easily include a pressure gradient in the analysis if we assume it varies as $1/X$. Since we integrate the pressure gradient over the length of the boundary layer, the exact dependence on X should not be crucial. Specifically, we substitute:

$$p_x=-\Sigma/\delta^2 x \tag{28}$$

into Eq. 2 and discard the viscous term that is $O(\delta^2)$. The dimensionless constant Σ is as yet undetermined. The analysis proceeds as before, and Eq. 14 becomes:

$$F_{zzz}+\frac{1}{2}FF_{zz}+\Sigma=0 \tag{29}$$

The analysis again proceeds as before, with Eq. 20 becoming:

$$\zeta=2\sqrt{\frac{15}{3+2\varphi}}\Big/\sqrt{1-\frac{30\Sigma}{(1-\varphi)(3+2\varphi)}} \tag{30}$$

and Eq. 22 becoming:

$$\frac{L}{D}=\frac{3}{20}\frac{(3+2\varphi)}{(1+2\varphi)^2}\left[1-\frac{30\Sigma}{(1-\varphi)(3+2\varphi)}\right]\left(\frac{\rho q}{\mu}\right) \tag{31}$$

Finally, we estimate Σ by an overall balance of X-momentum over the control volume between sections A-A and B-B in Figure 1:

$$\frac{\rho S^2 D}{F(\zeta)}\int_0^\zeta F_z^2 dz-\rho S^2 D\varphi=-\frac{2\rho S^2 D}{F(\zeta)}F_{zz}(0)+2\sigma[1-\sin(\alpha)] \tag{32}$$

These terms are the X-component of the momentum flux across section B-B, the X-component of momentum flux across section A-A, the integral of the shear stress on the substrate from the contact line to section B-B, and the net surface tension force. This last term is uncertain because the dynamic contact angle and the slope of the interface at section B-B are unknown; as an approximation we take a dynamic contact angle of 180° and an interface slope of 0°. To obtain a simple result, we use an integral form of Eq. 29 to evaluate the first term of Eq. 32:

$$\int_0^\zeta F_z^2 dz=-2F_{zz}(0)+F(\zeta)F_z(\zeta)+2\Sigma\zeta \tag{33}$$

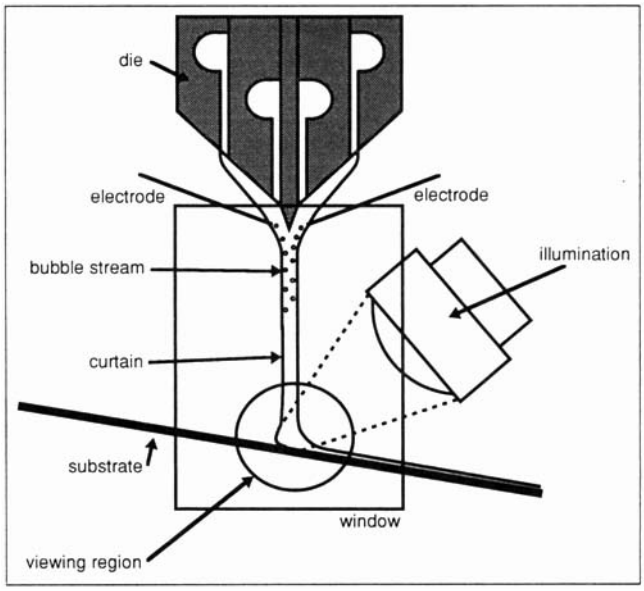

Figure 3. Experimental configuration.

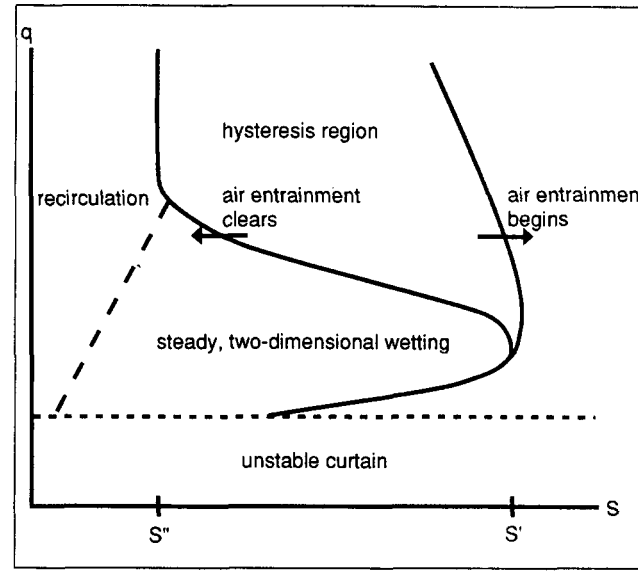

Figure 4. Flow regions.

The momentum balance then yields:

$$\Sigma = \frac{(1+2\varphi)}{3}\,\frac{(1-\sin(\alpha))}{We} \tag{34}$$

A wetting line position corrected for the effect of surface tension results when Eq. 34 is substituted into Eq. 31.

We present below experimental results indicating that this correction for surface tension improves the prediction of the wetting line position when surface tension effects become comparable to inertial and viscous effects. We can also compare the model with two finite-element computations by Kistler (1983) for the full set of equations and a Newtonian liquid. The flow conditions are $\delta = 1$, $\rho q/\mu = 2.5$, and a dynamic contact angle of 180°. For $\mu S/\sigma = 100$, the finite-element computation gives $l = 0.96$, and our model gives 1.12 (uncorrected) and 1.11 (corrected). This is surprisingly good agreement given the large value of δ. For $\mu S/\sigma = 3$, the finite-element computation gives $l = 0.66$, and our model gives 1.12 (uncorrected) and 0.62 (corrected).

Experimental Method

Observation of air entrainment

In our experiments, the liquid is pumped from pressurized containers and metered to a die (Figure 3) using precision gear pumps. Flow rates are accurate to ±3% over the range of the measurements. The delivery lines are water jacketed, and liquid temperatures are controlled to ±0.2°C. The die has four distribution cavities spanning the width of the flow. The liquid flows from each cavity near a narrow slot. The dimensions of the cavity and slot are chosen such that the pressure drop over the length of the slot is much larger than the pressure drop over the length of the cavity. In this manner, the liquid is distributed evenly across the width of the die for a broad range of Reynolds numbers and rheological properties.

The liquid exiting the die flows by gravity along the lower faces of the die, which are inclined to the horizontal, and then falls to form a vertical sheet of liquid, or curtain, several centimeters in height. The total flow is divided equally between the inclined surfaces to ensure a symmetric flow and a vertical curtain falling from the center element of the die.

In the curtain, the liquid is in free fall. Dynamic surface tension can be measured by creating and measuring standing waves (Antoniades et al., 1980). The width of the curtain is maintained by two vertical metal rods approximately 1.5 millimeters in diameter; in the absence of these, surface tension causes the curtain to contract as it falls. The curtain impinges upon the moving substrate, which is tilted at an angle α from horizontal.

The substrate is a 35-mm-wide web of poly(ethylene terephthalate), abbreviated as PET. The web is tensioned over a pair of rollers about 25 cm apart. For most of the data, the substrate has a previously applied subbing layer of gelatin. The web is driven by a customized drive system giving speeds accurate to within ±1% from less than 0.01 m/s to more than 10 m/s. The curtain is wider than the substrate to minimize edge effects. The wetting line and the first few centimeters of the coated layer are viewed from above and illuminated from the side with a strong, parallel beam of light provided by an Oriel 100 W lamp and power supply. Entrained air bubbles reflect the light and appear as bright points. The observations are recorded by a video camera (Prostab International) equipped with a gated image intensifier giving 50 images per second with a temporal resolution better than 0.1 ms. The video images together with recorded comments are stored for subsequent analysis using a JVC Umatic recorder. A FOR.A title generator and timer are used to superimpose speed, flow rate, and date/time data onto each image.

We plot our data as volumetric flow rate per unit width vs. coating speed (Figure 4). At too low a flow rate the curtain is unstable to sufficiently large disturbances (Brown, 1961; Lin, 1981), and the liquid can fall as spatially periodic streamers, as well as a sheet. The lower the flow rate, the more difficult it is to maintain a sheet, and we did not generally take data at flow rates below about 10^{-4} m^2/s.

At high flow rates and low speeds, a large heel, containing regions of recirculation, forms at the base of the curtain. In

extreme cases, the flow in the heel becomes unsteady and irregularly three-dimensional.

At sufficiently high speeds at any flow rate, the wetting line suddenly adopts an unsteady sawtooth shape, and air is entrained. At the highest flow rates, the speed at the onset of air entrainment either changes slowly with flow rate or approaches a constant value S''. This speed may be measured independently using high flow rates and a short curtain, a few millimeters in height, so that there is a large heel and the wetting line is isolated from the curtain. As flow rate is decreased from high values, the air entrainment speed departs from the curve for an isolated wetting line and increases. At a certain flow rate, the air-entrainment speed attains a maximum value, S', which can easily be an order of magnitude larger than S''. Speed then decreases to very low values as flow rate is reduced further, and the wetting line moves visibly downstream from the curtain.

At flow rates higher than that corresponding to S', there may be a region of air-entrainment hysteresis. Whether or not air entrainment occurs at a point in this region depends on how the point is reached. If, for example, air entrainment is produced by increasing speed at constant flow rate, it will not begin until the higher-speed boundary of the region is reached. If speed is then reduced, however, air entrainment does not clear until the lower speed boundary is reached. The difference between the two speeds can be as great as a few meters per second. An interesting hallmark of the hysteresis region is the possible occurrence of air entrainment over just some sections of the coated width. Strips of air entrainment then persist next to strips for which wetting is complete.

We focus on the lower-speed boundary of the hysteresis region. This is determined by increasing speed at constant flow rate until air entrainment occurs and then gradually decreasing the speed until all regions of air entrainment clear. Particularly when hysteresis is present, experimental points need to be repeated to give a good estimate of the lowest speed at which entrainment can persist. For all data reported here, each point was repeated up to four times.

The data have significant, inherent variability which hampers the analysis. When hysteresis is present, it certainly contributes to noise. We believe that variations in the chemical and physical properties of the substrate also play a role, but we do not know precisely what these are, much less how they can be measured and controlled over large areas. Random perturbations of the flow field may also contribute to the noise in the data. Clearly, it is a complicated response of the flow that is being observed.

Flow visualization

We visualize the impingement zone using an optical cross-sectioning technique (Schraub et al., 1965; Schweizer, 1988; Scriven and Suszynski, 1990). The small scale of the flow, a fraction of a millimeter, as well as the need to see past edge effects, make these observations challenging.

The visualization apparatus (Figure 5) is mounted beneath the die used for the air-entrainment observations. To avoid edge effects, we view the foot of the curtain near the center of the web. The thickness of the curtain is of order 300 μm and the required field of view is of the order 1 mm. To observe this region, we use a traveling microscope attached to a high-sensitivity CCD camera (Panasonic WV-BL200, 0.5 Lux sensitivity) linked to a JVC Umatic video recorder. This gives an effective field exposure time of 1/50 s, and a frame rate of 25 Hz. Typically, this system records continuously during the experiment and logs all observed flows. Single frames are captured from the videotape by an Apple Macintosh IIci computer equipped with a Data Translation frame grabber board. Automatix "Image Analyst" software enables measurements of the flow geometry, wetting line position and dynamic contact angle.

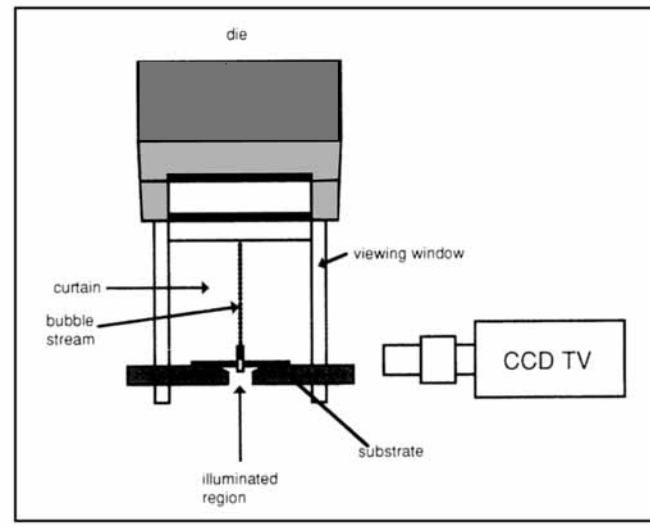

Figure 5. Configuration for optical cross-sectioning.

In order to observe the interfaces, small bubbles are released into the curtain by means of electrolysis (Schraub et al., 1965; Schweizer, 1988). Fine platinum cathodes (0.25 mm dia.) are adjusted to touch each interface near the die lip. The electrodes generate bubbles that are considerably smaller than the diameter of the wire used. Typically, a power supply providing up to 30 V and 10 mA is required; the exact voltage and current depend upon the conductivity of the liquid and the placement of the electrodes. The lighting of the bubble stream is crucial since it is necessary to obtain a high contrast between the bubbles and the surrounding liquid. To achieve this, a high-intensity source of white light is focused at the foot of the curtain in a darkfield mode; we use a Dolan-Jenner 180 light source equipped with a 200-W quartz halogen lamp. The lamp is focused onto the entrance of a fiber-optic bundle, the exit of which is arranged as a strip. The strip is focused onto the region of the bubble stream at the foot of the curtain using a Nikkor f1.2, 50-mm lens. This arrangement optically sections the flow and minimizes stray light so that we see only the curtain at the plane of the bubbles.

Edge effects pose problems. Viscous drag on the windows reduces the local velocity at which the curtain impinges onto the substrate. Air entrainment therefore occurs at a significantly lower speed adjacent to the windows. This carries the wetting line downstream and restricts our view of the center of the curtain. To overcome these effects, we alter the flow near the edges. A gap of approximately 6 mm is left between the windows and the edges of the substrate, and then to each window a horizontal platform is connected just below the plane of the substrate. Liquid accumulating on the platform allows a clear view of the wetting line. In some cases, extra liquid must be provided. This is achieved by placing small dies behind

Table 1. Rheological Properties

μ_0 mPa s	$\lambda \times 10^4$ s^{-1}	n	Notes
140	130	0.67	Dextran
33	0.31	0.66	PVA
59	14	0.73	PVP
51	——	1.0	PVP, K-30
51	5.3	0.85	PVP, K-60
55	40	0.68	PVP, K-90
50	19	0.86	High MW Gelatin
50	50	0.76	Microgel
—	see text	0.85	Bone Gelatin

the curtain to immerse both the edges of the substrate and the horizontal platforms. We have confirmed that the extra liquid does not feed into the observation area at the center of the curtain by comparing air-entrainment speeds both with and without the extra liquid.

Experimental Results

Rheological parameters

The liquids studied include aqueous solutions of poly(vinyl pyrrolidone), abbreviated PVP; dextran; poly(vinyl alcohol), abbreviated PVA; bone gelatin; and a microgel. The rheological parameters of these liquids are listed in Table 1 and were determined either with a Rheometrics System Four rheometer by the technique of Connelly and Greener (1985), or with a Bohlin VOR rheometer.

The majority of the reported data is for bone gelatin, the apparent viscosity of which was determined at high shear rates by Connelly, Contestable and Greener (1984), who also showed that the apparent viscosity data for different gelatin concentrations can be made to lie on a master curve by shifting the data in shear rate. Based on their work and our own measurements, we adopt the following values for the rheological parameters:

$$n = 0.85$$
$$\lambda = 1.55 \times 10^{-9} (\mu_0/w)^2 \qquad (35)$$

Here, λ has units of seconds, μ_0 has units of mPa·s, and w is the weight fraction of gelatin. The Newtonian viscosity at low shear rates is estimated from the following equation:

$$\mu_0 = 0.951\, e^{28.1w} \quad (w > 0.05) \qquad (36)$$

Correlating air-entrainment data

For a given liquid, impingement speed and inclination angle of the substrate, the air-entrainment speeds are determined experimentally at several flow rates (Figure 4). The first step in processing the data is to compute the relative wetting line position l, using Eq. 24. Although this equation is approximate and has a limited range of validity, it appears to have general utility; in other words l, as defined by Eq. 24, is a useful dimensionless parameter for correlating data. At least when δ is small, it may be considered to determine accurately the position of the dynamic wetting line. The next step in processing the data is to normalize the speed at which air entrainment clears by dividing by the maximum speed, S', which is shown below to depend upon the impingement speed of the curtain and inclination angle of the substrate.

When the original q-vs.-S plots are replaced by plots of l vs. S/S', the air-entrainment curves for each liquid at various impingement speeds and inclination angles collapse to one curve. We refer to the value of l at which S is maximum as the optimum relative wetting line position and use the notation l'. However, the curves so obtained for different liquids do not superimpose. To produce a master curve, it is necessary to plot l/l' against S/S'. We defer to later the dependence of l' on the properties of the liquid.

A straightforward averaging process yields the master curve from the air-entrainment data. We sort the data into seven ranges for S/S': 0.35–0.45, 0.45–0.55, 0.55–0.65, 0.65–0.75, 0.75–0.85, 0.85–0.95 and 0.95–1.0. Because the master curve is double-valued, having an upper section for $l/l' > l$ and a lower section for $l/l' < l$, fourteen groupings of data result. The data in each grouping are averaged, and the sample standard deviation is computed to indicate scatter (the data also vary because a curve is being estimated). The average value obtained for each grouping estimates the value of l/l' at the midpoint of the range for S/S'. Thus, the master curve (upper and lower branches) is determined for values of S/S' of 0.4, 0.5, 0.6, 0.7, 0.8, 0.9 and 0.975.

Table 2a. Master Curve—Gelatin

S/S'	l/l'	s.d.	% s.d.	Points
0.500	3.63	0.63	17	6
0.600	2.78	0.45	16	20
0.700	2.09	0.32	15	15
0.800	1.81	0.38	21	29
0.900	1.59	0.34	21	44
0.975	1.20	0.12	10	35
1.000	1.00	—	—	—
0.975	0.85	0.09	10	18
0.900	0.80	0.12	15	28
0.800	0.71	0.15	21	16
0.700	0.69	0.20	29	14
0.600	0.72	0.23	32	8
0.500	0.69	0.12	17	6
				—
				243

Table 2b. Data on PET Substrate: Subbed or Unsubbed with Gelatin

μ_0 mPa·s	α deg	H m	Notes
21	0	0.102	subbed
21	0	0.254	" "
21	45	0.102	" "
21	45	0.254	" "
22	0	0.060	unsubbed
65	0	0.060	subbed
65	0	0.102	" "
65	45	0.102	" "
65	45	0.254	" "
220	0	0.102	unsubbed
220	0	0.201	" "
220	0	0.254	" "
550	0	0.201	" "
600	0	0.356	" "

Table 3a. Master Curve—Other Polymers

S/S'	l/l'	s.d.	% s.d.	Points
0.500	3.94	0.86	22	2
0.600	2.42	0.22	9	3
0.700	2.36	0.32	14	7
0.800	1.65	0.36	22	10
0.900	1.39	0.28	20	10
0.975	1.23	0.14	11	8
1.000	1.00	—	—	—
0.975	0.90	0.05	5	6
0.900	0.85	0.02	3	5
0.800	0.79	0.02	3	3
0.700	0.81	0.08	9	2
0.600	0.78	0.02	3	2
0.500	0.85			1
				—
				60

The results of this process for the data for bone gelatin are given in Table 2, and for three other polymers in Table 3. Note that the estimates in Tables 2 and 3 are close, and this suggests that the data fall on a master curve that is applicable to predominantly pseudoplastic liquids.

Some of these data are plotted in both dimensional and reduced form to illustrate this result. Figure 6 shows dimensional data for aqueous gelatin for two viscosities and different combinations of curtain height and substrate inclination angle. Air-entrainment speed varies markedly with flow rate and depends also on impingement speed. Note that S' increases with height, and that the curves shift to lower flow rates as height is increased. The curves also appear to have the same general shape and thereby suggest the existence of a master curve. These and additional data for the two viscosities are plotted in reduced form in Figure 7. The estimated master curve is also shown. Finally, reduced data for 59 mPa·s aqueous PVP at three curtain heights are plotted in Figure 8 along with the master curve, which applies well to these data also.

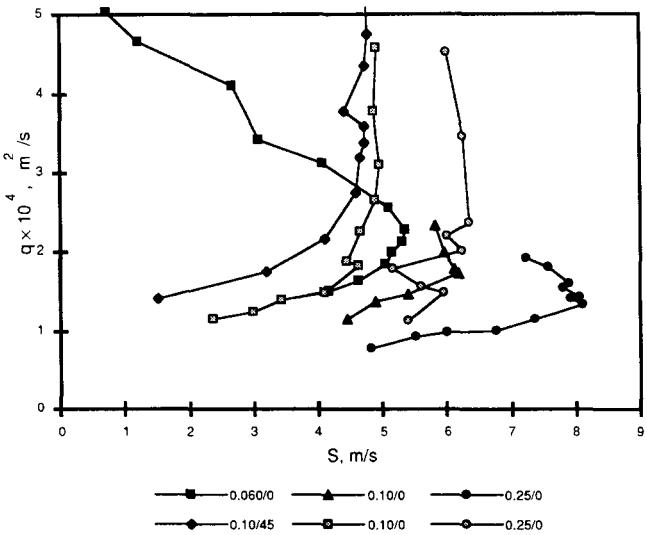

Figure 6. Data for the clearing of air entrainment plotted as volumetric flow rate per unit width vs. speed.

Aqueous solutions of bone gelatin have viscosities of 63 mPa·s (filled symbols) and 220 mPa·s (open symbols). The legend gives H in meters followed by α in degrees.

Table 3b. All Data on PET Substrate Subbed with Gelatin

μ_0 mPa·s	α deg	H m	Notes
140	0	0.102	Dextran
33	0	0.102	PVA
59	0	0.060	PVP
59	0	0.102	PVP
59	0	0.254	PVP

Optimum relative wetting line position

Our experiments have shown that the optimum relative wetting line position, as calculated from Eq. 22, depends upon the apparent viscosity in the boundary layer. Specifically, it depends linearly upon the reciprocal of apparent viscosity. The data used to determine the relationship cover several polymeric solutions and a broad range of impingement angle and impingement speed (the data are available as a supplement). The 67 data points are plotted in Figure 9. In the limit of high viscosity, l' appears to be constant. The relationship obtained by fitting the data is:

$$l' = 0.280 + 14.2/\mu \tag{37}$$

Here μ is in mPa·s, and the data cover apparent viscosities for the boundary layer between 8 and 220 mPa·s. As yet, we do not have an explanation for this result. The data are in-

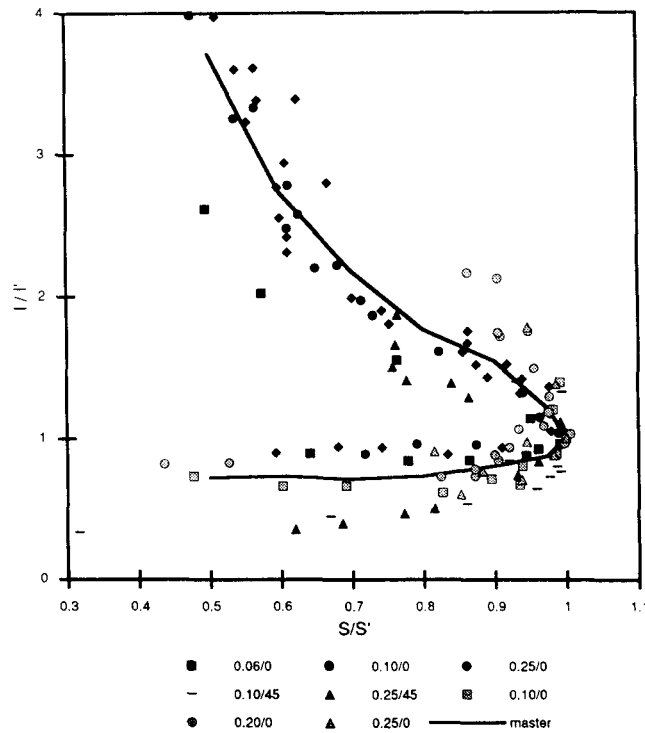

Figure 7. Data for the clearing of air entrainment plotted as normalized relative wetting line position vs. normalized speed.

Aqueous solutions of bone gelatin have viscosities of 63 mPa·s (filled symbols) and 220 mPa·s (open symbols). The legend gives H in meters followed by α in degrees. The master curve is also shown.

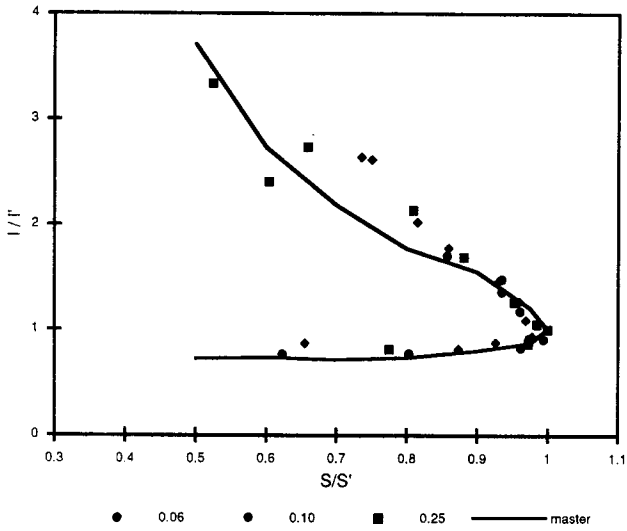

Figure 8. Data for the clearing of air entrainment plotted as normalized relative wetting line position vs. normalized speed.

Aqueous solution of PVP has a viscosity of 59 mPa·s. The legend gives H in meters, and α is 0°. The master curve is also shown.

adequate to determine a possible dimensionless relationship; it is possible that the properties of air are involved, as well as surface tension and surface properties of the substrate. We also note that Eq. 37 would be affected little were l' calculated from Eq. 31 rather than Eq. 22; this is because the Weber number is large at the high values found for S', and so surface tension has little effect on boundary-layer length.

Maximum air-entrainment speed

For each set of air-entrainment data for the variation of S with q, there is a maximum speed, S' (Figure 4), which we use to normalize the other speeds. We interpret this condition

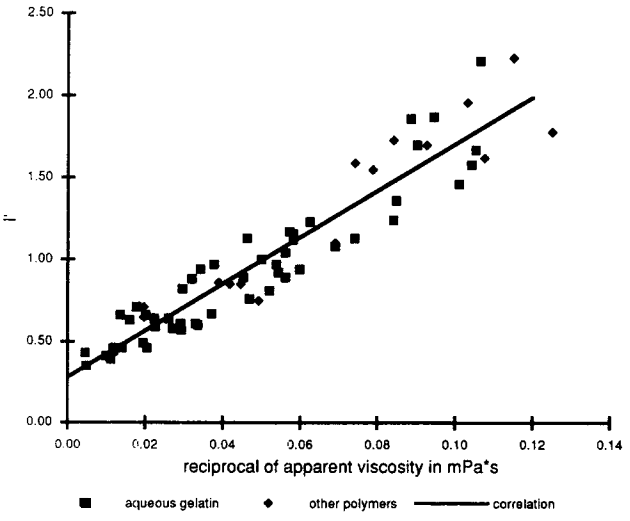

Figure 9. Data for optimum relative wetting line position vs. the reciprocal of apparent viscosity in mPa·s.

The line through the data is Eq. 37.

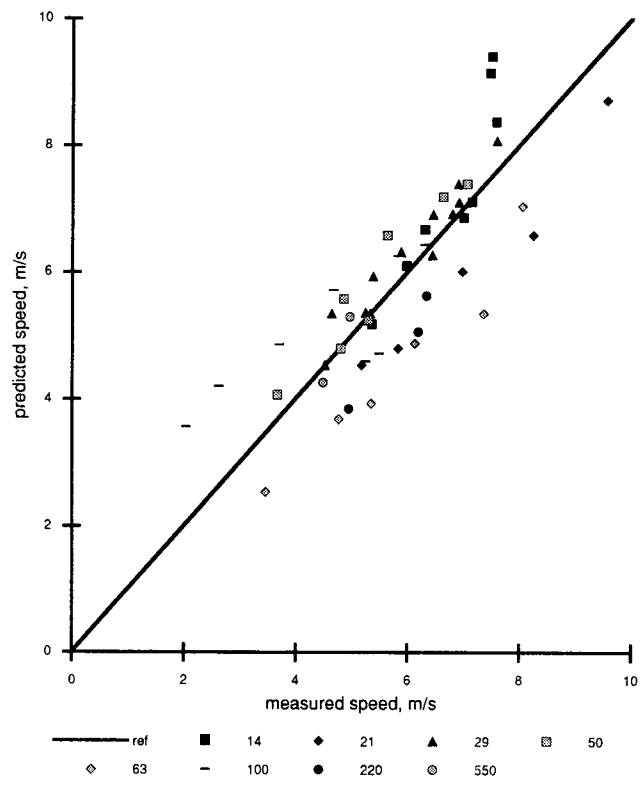

Figure 10. Data for the maximum wetting speed vs. the prediction of Eq. 38.

The legend gives low-shear viscosity in mPa•s.

as the most favorable for hydrodynamic assist of dynamic wetting, and so it is of particular interest.

Air entrainment begins when the macroscopic contact angle approaches 180°. It is not yet possible to make tenable predictions of the onset of air entrainment, because existing theories are incomplete. So, our main objective is to present reasonable correlations of the data. The basis for the correlations offered is our finding that U and α affect S' through the quantity $U\cos(\alpha)$. In other words, S' depends upon the component of curtain velocity normal to the substrate.

One way to correlate the data is suggested by a modified form of the molecular-kinetic theory of dynamic wetting (Blake, 1988). As a first attempt at extending that theory to capillary numbers above about 0.1, where hydrodynamic effects appear to be assisting wetting line advance, Blake (1988) has added a viscous driving force. As it stands, the modified theory can be applied only to a Newtonian liquid because the viscosity appearing as part of the driving force term is the actual viscosity of the liquid in the immediate vicinity of the wetting line. However, if the shear-rate dependence of viscosity for a polymer solution is modeled using Eyring theory (Glasstone et al., 1941), and if the characteristic speed of liquid approaching the wetting line is taken to be $U\cos(\alpha)$, then the modified theory suggests that $\mu_0 S'$ is proportional to $\mu_0 U\cos(\alpha)$ raised to a power. A detailed derivation will be given in a subsequent publication. Trying this leads to:

$$S' = 8.09\frac{(U\cos(\alpha))^{0.81}}{\mu_0^{0.19}} \quad (\mu_0 > 14 \text{ mPa·s}) \qquad (38)$$

In this equation, S' and U have units of m/s, and μ_0 units of

mPa·s. In Figure 10, S' as predicted by Eq. 38 is plotted against the measured values. The theory constrains the exponents in the numerator and denominator to sum to unity, but if this constraint is dropped and the general form of Eq. 38 is tried, the result is only slightly changed:

$$S' = 7.96 \frac{[U\cos(\alpha)]^{0.66}}{\mu_0^{0.17}} \tag{39}$$

According to Eq. 38, S' increases as the component of curtain speed normal to the substrate increases and decreases as low-shear viscosity increases. It is well established for plunging experiments with Newtonian liquids that air-entrainment speed varies inversely with viscosity to the 0.7 power (Gutoff and Kendrick, 1982; Burley and Jolly, 1984), and so an inverse dependence of S' on μ_0 is not surprising. There is no similar precedent for the effect of the impingement speed.

A second proposal for correlating the data comes from our observation that, for a given low-shear viscosity, the dependence of S' on $U\cos(\alpha)$ can reasonably be described by a straight line, at least over the range of the data. The lines for different viscosities appear to have different intercepts but the same slope. The result of this approach is:

$$S' = 2.08[U\cos(\alpha)] + \frac{10.7}{\mu_0^{0.4}} \tag{40}$$

This expression fits the data as well as Eq. 38.

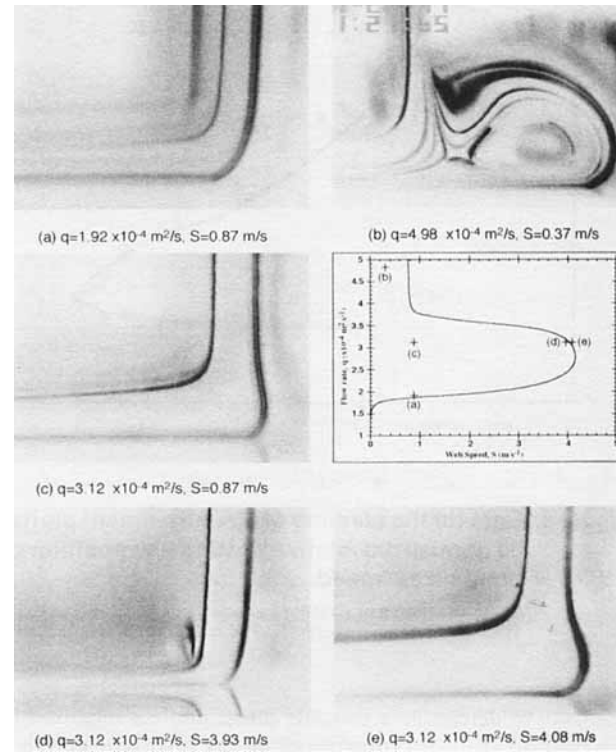

Figure 11. Optical cross sections for aqueous gelatin with $\mu_0 = 63$ mPa·s, $H = 0.03$ m and $\alpha = 0°$.

Flow visualization

Flow visualization supports our physical picture of flow and hydrodynamic assist in curtain coating. To illustrate these results, we present five cross-sections from the flow of 68 mPa·s aqueous gelatin. The curtain height is 3 cm and the substrate inclination angle is 0°. Figure 11d shows the flow just prior to the onset of air entrainment at approximately the flow rate at which the maximum speed is obtained. The wetting line is indeed confined beneath the curtain. The computed relative wetting line position, uncorrected for surface tension, is 0.60, and that corrected for surface tension is 0.51. These compare favorably with the measured value of 0.48. Figure 11e shows the flow at a slightly higher speed where air entrainment is occurring. The air film reduces the drag of the substrate; consequently, the apparent wetting line is displaced upstream, and the thickness of the layer downstream of the curtain increases. Figure 11c is for the same flow rate but a much slower speed. For this case the computed relative wetting line position is 1.9 (uncorrected) and 0.51 (corrected). Although the correction for surface tension brings the prediction in closer accord with the measured value of 0.86, the value of δ is 0.88, and so the condition is likely beyond the limits of the theory. Figure 11a is for the same speed but a lower flow rate, and the condition is on the edge of air entrainment. The measured relative wetting line position is -0.04, and those computed are 1.2 (uncorrected) and -0.2 (corrected). Finally, Figure 11b shows the profile for a high flow rate and a low speed. There is a large heel at the base of the curtain containing two regions of recirculation. At this high flow rate, air entrainment occurs at a speed of just 0.9 m/s.

We have measured the relative wetting line position for 15% bone gelatin, having a low-shear viscosity of 63 mPa·s, for a curtain height of 3 cm and a substrate inclination angle of 0°. At each of four flow rates, speed was increased to the air-entrainment boundary. The flow rates and speed ranges were: 3.74×10^{-4} m²/s, 0.77–1.47 m/s; 3.12×10^{-4} m²/s, 0.82–3.75 m/s; 2.60×10^{-4} m²/s, 0.76–2.97 m/s; and 2.02×10^{-4} m²/s, 1.06–1.40 m/s. The speed ratio δ ranged from 0.21 to 1.0, and the inverse Weber number from 0.051 to 0.28. These conditions are not completely ideal for testing the theory quantitatively but are representative of what we can visualize.

The results are plotted in Figure 12. Calculated values of the relative wetting line position are shown both with and without the surface tension correction; clearly surface tension has a substantial effect in many cases, and the correction markedly improves agreement with the experimental values. Also identified in the figure are those points for which δ is below 0.5 and the inverse Weber number is below 0.116; the correction for surface tension matters the least for these points.

The observation which comes closest to meeting the restrictions of the theoretical analysis has a speed ratio of 0.21 and an inverse Weber number of 0.051. The measured relative wetting line position is 0.54, that calculated without the surface tension correction is 0.67, and that calculated with the surface tension correction is 0.56.

Concluding Remarks

The maximum speed of dynamic wetting for an impinging curtain is affected by more than an order of magnitude by macroscopic hydrodynamic parameters including flow rate and

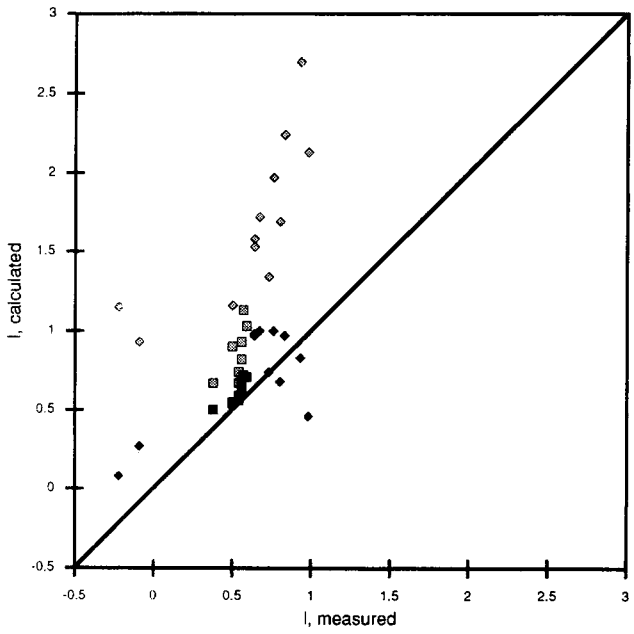

Figure 12. Calculated values of the relative wetting line position vs. measured values for aqueous gelatin with $\mu_0 = 63$ mPa·s, $H = 0.03$ m, and $\alpha = 0°$.

Computed values corrected for the effect of surface tension are represented by filled symbols; values uncorrected are represented by open symbols. For the square symbols, δ is below 0.5 and the inverse Weber number is below 0.116.

the impingement speed and angle. Flow visualization shows that the apparent dynamic contact angle is affected as well. It is worth noting that the two substrates we used were indistinguishable; possibly hydrodynamic effects are becoming dominant. Gutoff and Kendrick (1982) similarly found it difficult to distinguish smooth substrates in plunging experiments.

The model presented here is far from complete. To compensate for this, we employ extensive experimentation and flow visualization. Although the main results are semiempirical, they are useful and suggestive for further theoretical development. Until the physics of dynamic wetting becomes clear and quantitative, applications must rely heavily on experimental findings.

In particular, macroscopic hydrodynamics must be more thoroughly reconciled with events on the molecular scale at the dynamic contact line. Regardless of the model for dynamic wetting, it is necessary to specify a contact angle that may very well come from nonequilibrium thermodynamics.

Acknowledgment

Much of the experimental data was obtained by R. A. Dobson, J. W. Fergie-Woods, J. W. Harrison, S. D. Morley, and B. D. Stich. M. Brache helped to develop the flow visualization technique. Some of the rheological measurements were made by R. Connelly.

Notation

D = final film thickness
F = function of z
G = gravitational acceleration
H = vertical length of curtain
l = relative wetting line position, $L\cos(\alpha)/W$
l' = relative wetting line position at S'
L = boundary layer length
n = power law index
p = dimensionless pressure scaled with ρU^2
P = pressure
q = volumetric flow rate per unit width
Re = Reynolds number, $\rho UD/\mu$
S = substrate speed
S' = air entrainment speed maximized over flow rate
S'' = air entrainment speed at high flow rates
u = dimensionless X-component of velocity scaled with S
v = dimensionless Y-component of velocity scaled with U
U = curtain impingement speed
U_0 = initial curtain speed
W = width of the curtain above the impingement point
We = Weber number, $\rho qS/\sigma$
x = dimensionless X coordinate scaled with W
X = coordinate
y = dimensionless Y coordinate scaled with D
Y = coordinate
z = $\sqrt{\mathrm{Re}/xy}$ similarity coordinate

Greek letters

α = inclination angle of substrate
$\dot{\gamma}$ = shear rate
δ = U/S
ζ = value of z at envelope of boundary layer
λ = relaxation time
μ = Newtonian or apparent Newtonian viscosity
μ_0 = low-shear viscosity
μ_∞ = high-shear viscosity
ρ = density
σ = surface tension
Σ = constant
φ = $\delta\sin(\alpha)$
ψ = stream function

Literature Cited

Antoniades, M. G., R. Godwin, and S. P. Lin, "A New Method of Measuring Dynamic Surface Tension," *J. Colloid Interf. Sci.*, **77**, 583 (1980).

Bird, R. B., R. C. Armstrong, and O. Hassager, *Dynamics of Polymeric Liquids: 1. Fluid Mechanics*, Wiley, New York (1987).

Blake, T. D., "Wetting Kinetics—How Do Wetting Lines Move?" Paper 1a AIChE Meeting, New Orleans (1988).

Blake, T. D., "Dynamic Contact Angles and Wetting Kinetics," in *Wettability*, Surfactant Science Series, J. Berg, ed., Marcel Dekker, New York (1993).

Blake, T. D., and J. M. Haynes, "Kinetics of Liquid/Liquid Displacement," *J. Colloid Interf. Sci.*, **30**, 421 (1969).

Blake, T. D., and K. J. Ruschak, "A Maximum Speed of Wetting," *Nature*, **282**, 489 (1979).

Blake, T. D., and K. J. Ruschak, "Wetting: Static and Dynamic Contact Lines," *Liquid Film Coating: Scientific Principles and their Technological Implications*, P. Schweizer and S. Kistler, eds., Chapman and Hall, New York, in press (1994).

Bracke, M., F. De Voeght, and P. Joos, "The Kinetics of Wetting: the Dynamic Contact Angle," *Prog. Colloid Polym. Sci.*, **79**, 142 (1989).

Brown, D. R., "A Study of the Behavior of a Thin Sheet of Moving Liquid," *J. Fluid Mech.*, **10**, 297 (1961).

Buonopane, R. A., E. B. Gutoff, and M. M. T. Rimore, "Effect of Plunging Tape Surface Properties on Air Entrainment Velocity," *AIChE J.*, **32**(4), 682 (1984).

Burley, R., and R. P. S. Jolly, "Entrainment of Air into Liquids by a High Speed Continuous Solid Surface," *Chem. Eng. Sci.*, **39**, 1357 (1984).

Burley, R., and B. S. Kennedy, "An Experimental Study of Air Entrainment at a Solid/Liquid/Gas Interface," *Chem. Eng. Sci.*, **31**, 901 (1976).

Burley, R., "Air Entrainment and the Limits of Coatability," *JOCCA*, **5**, 192 (1992).

Cherry, B. W., and C. M. Holmes, "Kinetics of Wetting of Surfaces by Polymers," *J. Colloid Interf. Sci.*, **29**, 174 (1969).
Connelly, R. W., B. A. Contestable, and J. Greener, unpublished data (1984).
Connelly, R. W., and J. Greener, "High-Shear Viscometry with a Rotational Parallel-Disk Device," *J. Rheol.*, **29**, 209 (1985).
Cox, R. G., "The Dynamics of the Spreading of Liquids on a Solid Surface. Part 1. Viscous Flow," *J. Fluid Mech.*, **168**, 169 (1986).
de Gennes, P. G., X. Hua, and P. Levinson, "Dynamics of Wetting: Local Contact Angles," *J. Fluid Mech.*, **212**, 55 (1990).
Dussan V., E. B., "The Moving Contact Line: the Slip Boundary Condition," *J. Fluid Mech.*, **77**, 665 (1976).
Dussan V., E. B., "On the Spreading of Liquids on Solid Surfaces: Static and Dynamic Contact Angles," *Ann. Rev. Fluid Mech.*, **11**, 371 (1979).
Glasstone, S., K. J. Laidler, and H. J. Eyring, *The Theory of Rate Processes*, McGraw-Hill, New York (1941).
Gutoff, E. B., and C. E. Kendrick, "Dynamic Contact Angles," *AIChE J.*, **28**, 459 (1982).
Hansen, R. J., and T. Y. Toong, "Dynamic Contact Angle and its Relationship to Forces of Hydrodynamic Origin," *J. Colloid Interf. Sci.*, **37**, 196 (1971).
Hocking, L. M., and A. D. Rivers, "The Spreading of a Drop by Capillary Action," *J. Fluid Mech.*, **121**, 425 (1982).
Huh, C., and S. G. Mason, "The Steady Movement of a Liquid Meniscus in a Capillary Tube," *J. Fluid Mech.*, **81**, 401 (1977).
Inverarity, G., "Dynamic Wetting of Glass Fibre and Polymer Fibre," *Br. Polym. J.*, **1**, 245 (1969).
Kistler, S. F., "The Fluid Mechanics of Curtain Coating and Related Viscous Free Surface Flows with Contact Lines," PhD Thesis, Univ. of Minnesota, Minneapolis (1983).
Lin, S. P., "Stability of a Viscous Liquid Curtain," *J. Fluid Mech.*, **104**, 111 (1981).
Miyamoto, K., "On the Mechanism of Air Entrainment," *Ind. Coating Res.*, **1**, 71 (1991).
Mues, W., J. Hens, and L. Boiy, "Observation of a Dynamic Wetting Process Using Laser-Doppler Velocimetry," *AIChE J.*, **35**, 1521 (1989).
Perry, R. T., "Fluid Mechanics of Entrainment through Liquid-Liquid and Liquid-Solid Junctures," PhD Thesis, Univ. of Minnesota, Minneapolis (1967).
Petrov, P. G., and J. G. Petrov, "A Combined Molecular-Hydrodynamic Approach to Wetting Kinetics," *Langmuir*, **8**, 1762 (1992).
Sakiadis, B. C., "Boundary-Layer Behavior on Continuous Solid Surfaces," *AIChE J.*, **7**, 26 (1961a).
Sakiadis, B. C., "Boundary-Layer Behavior on Continuous Solid Surfaces: II. The Boundary Layer on a Continuous Flat Surface," *AIChE J.*, **7**, 221 (1961b).
Schraub, F. A., S. J. Kline, J. Henry, P. W. Runstadler, and A. Littell, "Use of Hydrogen Bubbles for Quantitative Determination of Time-Dependent Velocity Fields in Low Speed Water Flows," *Trans. ASME J. Basic Eng.*, **87**, 429 (1965).
Schweizer, P. M., "Visualization of Coating Flows," *J. Fluid Mech.*, **193**, 285 (1988).
Scriven, L. E., and W. J. Suszynski, "Take a Closer Look at Coating Problems," *Chem. Eng. Prog.*, **86**(9), 24 (1990).
Seebergh, J. E., and J. C. Berg, "Dynamic Wetting in the Low Capillary Number Regime," *Chem. Eng. Sci.*, **47**, 4455 (1992).
Teletzke, G. F., H. T. Davis, and L. E. Scriven, "Wetting Hydrodynamics," *Rev. Phys. Appl.*, **23**, 989 (1988).
Voinov, O. V., "Hydrodynamics of Wetting," *Fluid Dynamics*, **11**, 714 (1976).

Manuscript received Mar. 18, 1993, and revision received June 25, 1993.